




**Pulsation mechanism of a Taylor cone under a single pulse voltage**Jin-bo Cheng , Qi-you Liu , Li-jun Yang\*, Jun-xue Ren, Hai-bin Tang , and Qing-fei Fu<sup>†</sup>  
*School of Astronautics, Beihang University, Beijing 100191, China*

Luo Xie

*School of Marine Science and Technology, Northwestern Polytechnical University,  
Xi'an Shaanxi 710072, China*

(Received 25 July 2022; accepted 12 December 2023; published 8 January 2024)

Electrospray has the advantages of high efficiency and accurate thrust, which can meet the requirements of microsatellites on micropropulsion systems, and it is a new type of microthrust system with great potential. Due to the stable characteristics of the cone jet, most of the existing research focuses on the steady electric field, while the response of the Taylor cone shape to the pulse voltage has vital application significance in the attitude control of the microthruster and the active control of the electrospray switch. Therefore, this paper focuses on the research on the response mechanism of the Taylor cone shape to a single pulse voltage. Based on experimental research, a high-speed camera is used to capture the time-series images of the Taylor cone, and a trigger connection is used to synchronously collect the atomization current under a single pulse disturbance voltage to assist in exploring the oscillation mechanism. The research shows that the pulsation of a Taylor cone under the action of a single pulse voltage has a strong coupling relationship with the conductivity and permittivity of the dielectric in the fluid, that is, the oscillation time has a strong consistency with the polarization charge relaxation time of the dielectric in the fluid.

DOI: [10.1103/PhysRevFluids.9.013701](https://doi.org/10.1103/PhysRevFluids.9.013701)**I. INTRODUCTION**

Electro-atomization is a method in which conductive liquids are broken and atomized into droplets under the combined action of higher electric field force ( $\sim$ kV) and hydrodynamic effects (including surface tension, viscous force, and aerodynamic force, etc.). It has the same physical mechanism with the concepts of electrohydrodynamics and electrojets. Due to better atomization effect and more effective regulation [1], it has been widely used in industrial fields, such as spray coating, inkjet printing, industrial dust removal and desulfurization, particle coalescence and separation, mass spectrometry analysis, etc. Meanwhile, based on the actual demand of aerospace attitude and orbit control technology for microthrust engines, the electrospray micropropulsion technology has been vigorously developed [2–5], that is, the very fine liquid charged particles are extracted through the capillary electrospray process, and then the charged particles are accelerated by the electric field to produce microinjection, so as to obtain thrust.

---

\*Also at Aircraft and Propulsion Laboratory, Ningbo Institute of Technology, Beihang University, Ningbo 315800, China.

<sup>†</sup>Also at Aircraft and Propulsion Laboratory, Ningbo Institute of Technology, Beihang University, Ningbo 315800, China; fuqingfei@buaa.edu.cn

As early as 1600, William Gilbert observed and documented the electrohydrodynamic atomization process for the first time, known as electroatomization or electrospray, and noted that electric fields could significantly improve difficult atomization [6]. In 1750 Jean-Antoine (Abbé) Nollet, a French priest and physicist known as the father of the experiment of electroatomization, reported the earliest electrospray phenomenon, proving that water flowing out of the container would be atomized when the container was powered on and close to the earth pole [7]. In 1896 Lord Raleigh [8] theoretically evaluated the maximum amount of charge that a certain mass of liquid droplets can carry, known as the “Raleigh limit.” This charged droplet-breaking mechanism dominated by Rayleigh limit is developed from the long strip jet, and a symmetrical jet is formed at both ends of the long strip, which is called the Rayleigh jet. Rayleigh instability also occurs in the rupture of neutral droplets under a strong DC electric field [9]. In 1964 Taylor [10] established the balance between capillary force and electrostatic stress on an equipotential cone, resulting in an accurate half cone angle of  $49.3^\circ$ , hence the name Taylor cone.

The study of electroatomization begins with a stable cone jet. In 1917 Zeleny [11] proved through a large number of experiments that the stable cone jet can appear and maintain only at a specific voltage and flow. Angamma *et al.* [12] used polyethylene oxide as the working fluid to conduct experimental research and numerical simulation on the double-nozzle electroatomization, obtained the spatial electric field distribution of the double nozzle system, and experimentally investigated the mechanism of the interaction of double-cone jets. Herrada *et al.* [13] proposed a robust and computationally efficient numerical scheme for simulating steady electrohydrodynamic atomization processes (electrospray). Gamero-Castaño *et al.* [14] solved numerically the equations of the leaky dielectric model applied to cone jets. A stable cone jet is of great value in practical application. However, due to the large voltage and small flow required to form a stable cone jet, the fluctuation of voltage and flow often occurs in practical operation. In view of this problem, many scholars have proposed many methods to help stabilize the cone jet. Cruz-Mazo *et al.* [15] made the cone jet maintain a more stable shape by applying annular air flow in the flow direction of the cone jet. Li *et al.* [16] used a nozzle structure similar to the ballpoint pen tip to study the cone jet and obtained the relationship between the droplet diameter, meniscus height, and applied voltage and flow rate. The nozzle with this special structure helps to reduce the viscous damping time and make the Taylor cone more stable. Morad *et al.* [17] designed a nozzle with an extended cap. In the experiment, it was found that the nozzle with this special structure made the jet more stable than the ordinary cylindrical nozzle. Gamero-Castaño *et al.* [18] used propylene carbonate and tributyl phosphate as working fluids to obtain the scaling law of minimum flow rate, Reynolds number, and characteristic radius, and qualitatively obtained the minimum flow rate change and its influencing process that affect the stability of cone jet. Gañán-Calvo *et al.* [19] studied multicoaxial stable cone jet. Wang *et al.* [20] brought the stable Taylor cone mode to the extreme and produced thousands of Taylor cones on the disk, which greatly improved the utilization of this mode in related fields.

Some scholars have conducted relevant research on the formation and stability analysis of the cone jet. As mentioned earlier, Taylor [10] was the first to conduct theoretical analysis and experimental verification on the formation of the cone-jet structure, and the basic characteristics of the Taylor cone angle in the experiment verified its calculation results. Agostinho *et al.* [21] studied the spray characteristics of a charged liquid. They referred to this mode as a simple jet. As the applied voltage increased, more and more charges accumulated on the droplets. Under the combined action of electric field force and surface tension, if the electric field force was high enough, the liquid meniscus could maintain a stable conical shape (Taylor cone). Jiang *et al.* [22] studied the formation of the cone jet in the electrospray process considering the space charge effects.

Regarding the stability of charged jets, in 1882 Lord Rayleigh [23] first obtained the dispersion equation of a completely conductor charged inviscid jet and pointed out that the surface charge would weaken the stability of the jet. Taylor [24] studied the stability of a water jet in an axial electric field by means of experiment and theory. Son and Ohba [25] addressed the classic needle-plate electroatomization experimental device, using the complete conductor hypothesis, derived the dispersion equation of water jet, studied the influence of the main parameters (potential distance

between needle and plate) that affect the magnitude of electric field force on the axisymmetric and nonaxisymmetric unstable modes, and compared with the experiment. In fact, for most electrohydrodynamic phenomena, it is unrealistic to assume that the fluid is a complete dielectric or a complete conductor, because for the real fluid, under the action of an axial electric field, even a small conductivity will make the fluid interface carry charge and interact with the axial electric field to produce tangential electric field force; therefore, the viscous force (the fluid must be moving) must be considered to balance the tangential electric field force [26] (the inviscid jet can use only the complete conductor or dielectric model). Melcher and Taylor [27] studied the convection phenomenon in the thin layer of liquid and droplets in the DC electric field and summarized the leaky dielectric model, that is, a dielectric with a certain conductivity has a tangential electric field force under the action of an electric field.

There are multiple modes in the electroatomization process, with the cone-jet mode being the most stable. However, under external factors such as voltage, electrode spacing, and flow rate, the Taylor cone often exhibits pulsations of different modes. Collins *et al.* [28] conducted detailed research on the transient development of the EHD tip jet through direct numerical simulation and experimental methods, and improved the scaling laws for predicting droplet size. Guan *et al.* [29,30] successively carried out numerical investigations on a high-frequency ( $\sim 1$  kHz) pulsating electrohydrodynamic jet at low electric Bond numbers, and EHD jet printing under constant and step change of electric voltages. Mohammadi *et al.* [31] used a new numerical model which couples the fluid flow, the electric field distribution, and the movement of the electric charges under dynamic and transient conditions to simulate the formation of a droplet in an EHD printer under a pulsed electrical field. Jaworek *et al.* [32] studied the effect of viscosity on electroatomization and mainly carried out the experiment of the rupture of ethylene glycol aqueous solution under the combined action of an electrostatic field and alternating electric field. Yeo *et al.* [33] proposed a new method of using high-frequency ( $> 10$  kHz) alternating electroatomization to generate electrically neutral microdroplets. They pointed out that, unlike the continuous formation of droplets at the end of the Taylor cone under the action of an electrostatic field, under the action of an alternating electric field, a resonant meniscus appeared at the nozzle, and then droplets were intermittently generated. The resonance frequency depends on the capillary-inertial oscillation time of the meniscus and the Maxwell-Wagner electric field force at the tip of the droplet. When the frequency of the applied electric field exceeds the resonance frequency, the wetting effect caused the liquid to adhere to the printhead. Subsequently, they pointed out that micron-scale, electrically neutral droplets can be generated by this high-frequency alternating electroatomization, which can be used in the field of biomaterial synthesis [34].

The process of electroatomization is essentially the combination of electrodynamics and hydrodynamics. The structure and dissociation properties of the molecular components of any liquid composition determine its electric properties, especially in the application of electrokinetic fluid and electrospray. The first is its electrical conductivity, and the second is its permittivity. The molecular dissociation process and the equilibrium constant of this process determine the mobility and concentration of liquid component ions, thus determining the electrical conductivity of the liquid. The polarity of a molecule is determined by its charge density distribution and its size. The ratio of the distance between the center of mass and the center of charge density to the molecular size determines the magnitude of the polarity of the molecule. The larger the ratio, the greater the polarity of the molecule and the permittivity of the liquid [35]. López-Herrera *et al.* [36] provide a high degree of accuracy solution to the complete electrokinetic structure of the steady Taylor cone-jet mode (TCJ), and consider a formulation with no interfacial adsorption of ions to calculate the strongly nonhomogeneous distribution of conductivity in the bulk. For low and moderate electrolytes and liquid permittivity up to 31.2 times  $\epsilon_0$ , Gañán-Calvo [37] proposed two simple scaling laws for the emitted current and jet diameter applicable to the stable cone-jet mode. In this scaling, the electric current  $I$  and the characteristic microjet radius  $R_0$  are both proportional to the square root of the emitted flow rate  $Q^{1/2}$ , and independent of the liquid permittivity  $\epsilon_l$ . Faraji *et al.* [38] used KCl solutions with different concentrations to focus on the influence of electrical

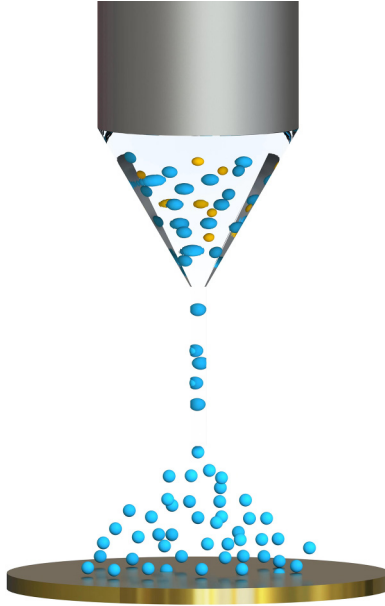


FIG. 1. Stable Taylor cone [39].

conductivity on the electric atomization modes and droplets. The results showed that compared with hydrodynamics, the atomization modes depended more on the liquid electrical conductivity. With the increase of conductivity, the strength of the applied electric field required for the formation of Taylor cone decreased, and the droplet size and liquid filament velocity decreased.

The charge relaxation time of a fluid is defined as the ratio of permittivity to electrical conductivity. By means of experiments, this paper explores the coupling relationship between the oscillation period of Taylor cone and the charge relaxation time of a fluid under the action of a single pulse voltage, selects five fluids with different charge relaxation times for the experiment, uses a high-speed camera to capture the time series image of the Taylor cone shape, and uses trigger connection to synchronously collect the atomization current under the single pulse voltage. The mechanism conjecture of our previous work [39] is well verified from the experimental aspect.

## II. EXPERIMENTAL SETUP AND METHODS

When liquid flows out of the charged metal capillary tube at a small flow rate, the liquid surface deforms under the action of a strong electric field. The higher the applied voltage, the stronger the electric field strength. When the electrostatic force on the liquid is balanced with the surface tension, the liquid surface forms a stable cone, the Taylor cone, as shown in Fig. 1. The liquid is pulled into a thin jet and then atomized, broken into small droplets, and the energy conversion between the potential energy and the surface energy and kinetic energy of the droplets is completed.

A single pulse voltage signal is applied to the stable Taylor cone, and the tip of the Taylor cone oscillates up and down for multiple periods at a certain frequency under the disturbance of a single period, as shown in Fig. 2.

### A. Experimental setup

The electroatomization experimental platform shown in Fig. 3 was built, which mainly includes a high-speed camera (FASTCAM SA-Z), green laser, stainless steel nozzle, copper disk electrode,

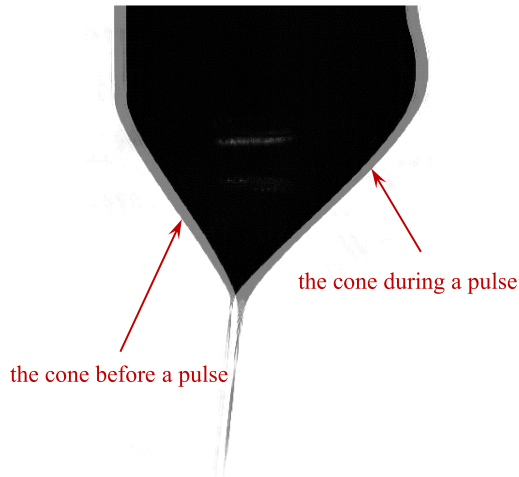


FIG. 2. Schematic diagram of the change of cone shape after applying a single pulse voltage.

fixed value resistor, syringe pump (LSP01-1BH), signal generator (UTG2062A), high-voltage amplifier (Trek 609E-6), data acquisition unit (DH5922D), etc.

The experimental system is divided into a flow supply system, electrical disturbance system, data acquisition system, and high-speed photography system.

The flow supply system uses a syringe pump to supply constant flow to the nozzle, and the syringe pump model is LSP01-1BH. It can be loaded with a sampler of  $10 \mu\text{l}$  to  $100 \text{ ml}$ . The linear velocity range is  $5 \mu\text{m}/\text{min}$  to  $130 \text{ mm}/\text{min}$ , and the linear velocity adjustment resolution is  $5 \mu\text{m}/\text{min}$ , and the stroke control accuracy error is less than or equal to  $\pm 0.5\%$ , which fully meets the flow requirements of this experiment.

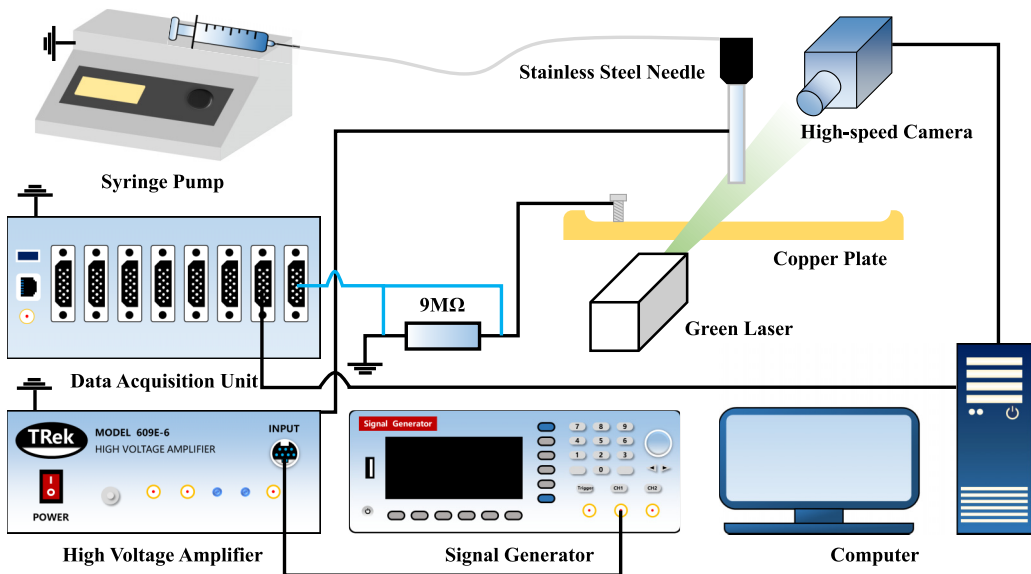


FIG. 3. Schematic diagram of electroatomization experimental platform.

The electrical disturbance system is composed of a signal generator and a high-voltage amplifier. The signal generator outputs a small disturbance voltage, which is amplified by the high-voltage amplifier and applied to the stainless-steel nozzle to make the liquid contact charged. The model of the signal generator is UTG2062A, which can output arbitrary waveform signals. The maximum arbitrary waveform length is 1 Mpts, the maximum sampling rate is 250 MS/s, the maximum output frequency is 60 MHz, the frequency resolution is 1  $\mu$ Hz, and the vertical resolution is 14 bits. The model of the high-voltage amplifier is Trek 609E-6, and its magnification is fixed at 1000, the input voltage range is 0  $\sim$   $\pm$  4 kV, the output current range is 0  $\sim$   $\pm$  20 mA, the output AC voltage frequency is less than 6 kHz, and the distortion rate is less than 1%. The pulse AC signal applied in the experiment is the AC signal superimposed under the DC voltage satisfying the stable cone jet. The results of the previous experimental research show that the voltage that meets the stable cone jet is within 4 kV, and the frequency requirement is much less than 6 kHz; thus the experimental instrument can meet the experimental requirements.

The data acquisition system uses a data acquisition unit to collect the atomization current signal, its model is DH5922D, and the continuous sampling frequency can achieve 32-channel synchronization, 256 kHz/channel. When using more than 32 channels, the sampling frequency is 128 kHz/channel. In the experiment, a copper plate (80 mm in diameter, 10 mm in thickness) was used as the collector to collect the charged atomized droplets, which flowed into the ground electrode (i.e., negative electrode) through the M $\Omega$ -level fixed-value resistor in series. The BNC interface is used between the acquisition process and the high-speed photography system to achieve synchronous triggering and synchronous acquisition; that is, the moment of single pulse application, current signal acquisition, and high-speed photography is the same moment.

The high-speed photography system adopts the FASTCAM SA-Z high-speed camera produced by Japanese Photron Company. Its photography performance reaches 20 000 fps/s under 1 million pixels (1024 $\times$ 1024 resolution), and the highest frame rate can reach 224 000 fps/s at low resolution. The minimum exposure time is 0.25  $\mu$ s, and it has multiple trigger modes such as start, center, random, and end, which can realize the synchronization of image acquisition and atomization current acquisition. The macro microscope lens (Leica Z16 APO) is used for shooting. Its apochromatic objective lens has improved image contrast, brightness, color fidelity, and image accuracy. In addition, due to the small amount of light entering the microscope, a green laser with a rated power of 3 mW was used as the light source in the experiment. The light is clear, the beam angle is large, and the straightness is high. The focus can be fixed, and the thickness of the light can be adjusted. Due to the high energy density of the laser and the little interference to the measurement of the atomization voltage, it is a good choice for the lighting source of the electroatomization system.

## B. Experimental working fluid

In this paper, five experimental fluids were used, namely, absolute ethyl alcohol, ethylene glycol, *n*-propanol, absolute ethyl alcohol salt solution with added sodium iodide, and a 50% ethanol water aqueous solution. We summarize the variable physical quantities introduced during the experimental process into a series of dimensionless electroatomization numbers using the Väschi-Buckingham theorem. Among them, electrical conductivity is a key parameter affecting the charge relaxation time, and it is generally sensitive to temperature. Therefore, this paper uses a DDSJ-308F conductivity meter with a DJS-0.01VT conductivity electrode for measurement. The measurement range of this conductivity electrode is 0–2  $\mu$ S/cm; the measurement results are recorded in Table I.

## C. Method of applying a single pulse disturbance voltage

In this paper the influence mechanism of the Taylor cone shape under a single pulse disturbance voltage is explored. Therefore, the DC voltage that can maintain a stable Taylor cone is used as the DC offset for applying the disturbance voltage. On this basis, disturbance voltages with different pulse widths and pulse heights are superimposed. Due to the exploration of the oscillation

TABLE I. Physical parameters of alcohol experimental fluids.

Experimental fluids	Electrical conductivity ( $\mu\text{S}/\text{cm}$ )	Relative permittivity (1)	Surface tension ( $\text{mN}/\text{m}$ )	Density ( $\text{kg}/\text{m}^3$ )	Viscosity ( $\text{mPa}\cdot\text{s}$ )
Absolute ethyl alcohol	0.003 (25.7)	24.1	22	789	1.19
Ethylene glycol	0.003 (25.8)	37	46.5	1113	17.32
<i>n</i> -propanol	0.002 (25.7)	20.1	24.5	804	2.256

mechanism of the Taylor cone, under the set conditions, the Taylor cone does not rupture, but only oscillates up and down. The schematic diagram of applying disturbance voltage is shown in Fig. 4.

#### D. Subpixel contour extraction algorithm

In order to explore the oscillation mechanism of Taylor cone under a single pulse voltage disturbance, this paper extracts the contour of Taylor cone diameter at a fixed position (actually taking the tip of the cone). The edge detection algorithm is used to obtain the boundary data of the cone jet from the experimental images. Most experimental studies on liquid jets use pixel-level algorithms to extract jet shape, but the accuracy of this method is limited by pixel grid points. Therefore, pixel-level methods are difficult to identify the small fluctuations at the tip of the Taylor cone. In order to solve the problem of detection precision, many subpixel methods have been proposed, which can achieve higher accuracy [40]. Subpixel methods have been applied to many fields, such as photogrammetry, spacecraft navigation, remote sensing, *et al.* [41,42]. In this paper a Zernike moments method presented by Ghosal is used to achieve subpixel-level edge detection, which has high accuracy and short run time [42–44]. For an experimental image, we first use a Canny operator to detect all pixel-level points [45]. Then, based on the points detected by the Canny operator, the precise positions are calculated using the Zernike moments operator. The schematic diagram of edge detection result for a cone jet is shown in Fig. 5.

### III. RESULT AND DISCUSSION

In the experiment a needle-plate electroatomization experimental device was used. For the five selected fluids, a stable Taylor cone can be formed under a certain DC voltage. During the experiment, after applying a single pulse disturbance voltage signal with different pulse widths and heights to the cone, the oscillation of the experimental fluid is mainly a continuous periodic oscillation, that is, the single pulse voltage disturbance causes multiperiod oscillation of the Taylor cone. However, ethylene glycol is limited by its physical parameters, and due to its large viscosity, it shows only one elongation and retraction of Taylor cone in the single period range of disturbance and does not form a multiperiod oscillation.

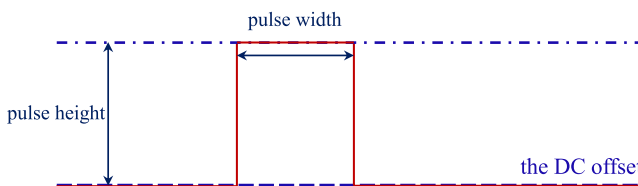


FIG. 4. Schematic diagram of applying a single pulse disturbance voltage.

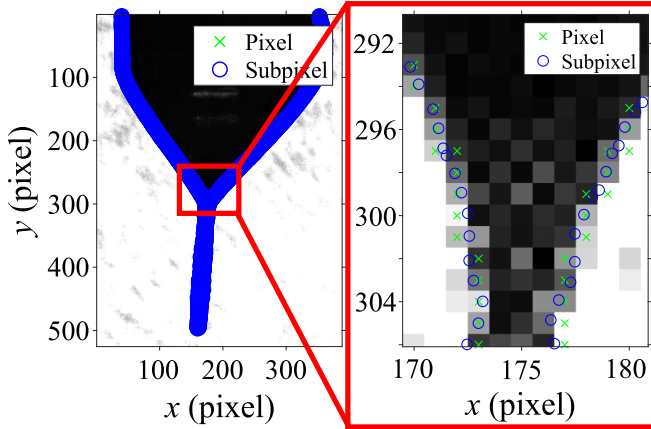


FIG. 5. Schematic diagram of subpixel-level contour extraction.

### A. Experimental results

As shown in Table II, the experimental parameters for five different fluids are listed. The table lists the stainless steel nozzle specifications used in the experiment, the distance between the nozzle outlet and the copper plate ( $D$ ), the stable flow rate ( $Q$ ), the corresponding DC voltage when forming a stable Taylor cone ( $U$ ), and all experimental conditions for the single pulse disturbance voltage.






As mentioned above, the selection of experimental conditions is to ensure that the Taylor cone remains complete under this disturbance form. This paper explores the oscillation mechanism of the complete Taylor cone under a certain disturbance.

TABLE II. Physical parameters of alcohol experimental fluids.

Experimental fluid	Nozzle specifications	$D$ (mm)	$Q$ ( $\mu\text{l}/\text{min}$ )	$U$ (kV)	Experimental conditions
Absolute ethyl alcohol	23 G (inner diameter 0.33 mm, outer diameter 0.63 mm)	2	7	2.85	Pulse widths 10 ms, 20 ms, 30 ms, 40 ms, 50 ms Pulse heights 100 V, 200 V, 300 V, 400 V
Ethylene glycol	23 G	2	14	3.75	Pulse widths 10 ms, 20 ms, 30 ms, 40 ms Pulse heights 60 V, 90 V, 120 V, 150 V
<i>n</i> -propanol	22 G (inner diameter 0.4 mm, outer diameter 0.7 mm)	2	1	3.2	Pulse widths 10 ms, 20 ms, 30 ms, 40 ms Pulse heights 100 V, 150 V, 200 V
Absolute ethyl Alcohol salt solution with added NaI	23 G	2	7	1.8	Pulse widths 10 ms, 20 ms, 30 ms, 40 ms Pulse heights 50 V, 100 V, 200 V
50% ethanol	23 G	2	7	2.1	Pulse widths 10 ms, 20 ms, 30 ms, 40 ms Pulse heights 50 V, 100 V, 150 V, 200 V
Aqueous solution					



TABLE III. Stable Taylor cone of experimental fluids under DC voltage.

Experimental fluids	absolute ethyl alcohol	ethylene glycol	n-propanol	absolute ethyl alcohol salt solution with added NaI	50% ethanol aqueous solution
stable Taylor cone experimental diagram					

The experimental pictures of five experimental fluids forming a stable Taylor cone under a certain DC voltage are shown in Table III.

Under the action of a single pulse disturbance voltage, the Taylor cone tip oscillates up and down for multiple periods. A subpixel level contour extraction algorithm is used to extract the diameter at a fixed position of the Taylor cone tip, and obtain the diameter oscillation diagram under different pulse widths and heights. Figure 6 shows the time series signal curves and its partial enlarged view extracted by five fluids under certain experimental conditions. (Due to the large amount of data, only some experimental conditions are shown in the table, and the postprocessing curves for the complete experimental conditions are shown in Appendix A.)

When no single pulse disturbance is applied, the Taylor cone remains stable, corresponding to a fixed diameter at the extraction position. When the disturbance signal is applied to the cone, the cone oscillates up and down, corresponding to the oscillation of the diameter. Therefore, the diameter signal curve first follows a straight line and then oscillates. The experimental results show that under the single pulse disturbance voltage, the oscillation period of the diameter exhibits a certain regularity. As the pulse height increases, the oscillation period gradually decreases, but the

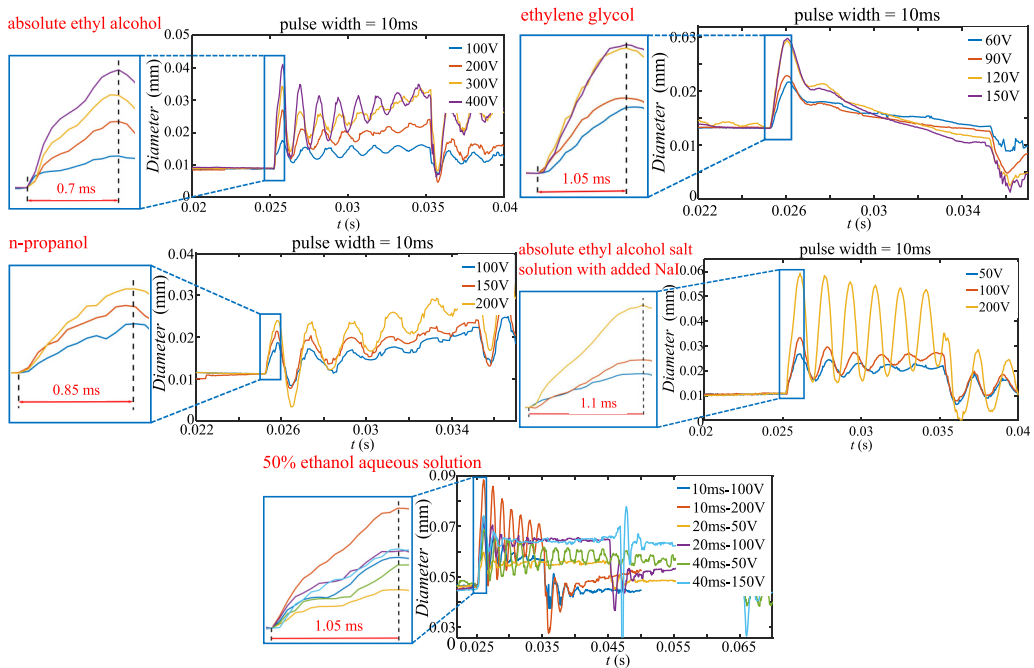


FIG. 6. Diameter oscillation diagram of experimental fluids under single pulse disturbance voltage.

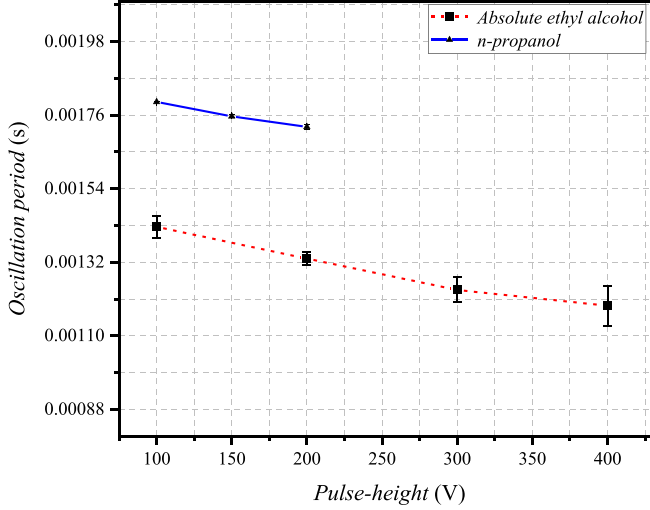


FIG. 7. Diagram of absolute ethyl alcohol and *n*-propanol diameter oscillation period with pulse height.

period does not change with the pulse width. Figure 7 shows the variation of the oscillation period of absolute ethyl alcohol and *n*-propanol with pulse height. Due to the difference in the physical properties of ethylene glycol, its viscosity is approximately 15 times that of absolute ethyl alcohol. Under the action of a single pulse waveform voltage, the potential energy input to the Taylor cone has been converted into internal energy and dissipated after a single oscillation, and only part of the energy is converted into the kinetic energy of its oscillation. The experimental results show that the diameter of ethylene glycol only increases and then decreases after being disturbed by a single pulse, and the absolute value of the decreasing slope increases with the increase of the pulse height, but the period of its single oscillation cannot be accurately determined. Except for ethylene glycol, the periodic characteristics of other fluids are consistent, and only absolute ethyl alcohol and *n*-propanol are shown in Fig. 7.

Interestingly, from the partial enlarged view of diameter oscillation shown in Fig. 6, it can be seen that the increasing time of the diameter oscillations of all fluids is a constant value, with absolute ethyl alcohol at 0.7 ms, ethylene glycol at 1.05 ms, *n*-propanol at 0.85 ms, absolute ethyl alcohol salt solution at 1.1 ms, and 50% ethanol aqueous solution at 1.05 ms. This constant value does not change with pulse height or pulse width (detailed data can be found in Appendix A). This partial enlarged view shows the situation only in the first oscillation period, and the subsequent oscillation periods have also been counted, and the obtained rules are consistent; the increasing time of the diameter oscillation is a constant value. Therefore, the variation of the oscillation period with the pulse height is reflected only in the descending section of the diameter oscillation.

Afterwards, we will explore the mechanism of Taylor cone oscillation using this invariant.

### B. Analysis of oscillation mechanism

Starting from the charge conservation equation,  $\frac{\partial \rho_e}{\partial t} + \vec{\nabla} \cdot (K\vec{E}) = 0$ , where  $\rho_e$  is the charge number density,  $K$  is the electrical conductivity of the fluid, and  $E$  is the electric field strength. Combined with the local relation of Gauss's theorem,  $\vec{\nabla} \cdot \vec{E} = \frac{\rho_e}{\epsilon}$ , where  $\epsilon$  is the permittivity of the fluid. The simultaneous solution can be obtained:

$$\rho_e = \rho_{e0} e^{-t/\tau_e}, \quad (1)$$

where  $\rho_{e0}$  is the initial charge density, and  $\tau_e = \epsilon/K$  is the charge relaxation time of the fluid. The Taylor cone reaches electrostatic equilibrium after a period of time in an electric field environment.

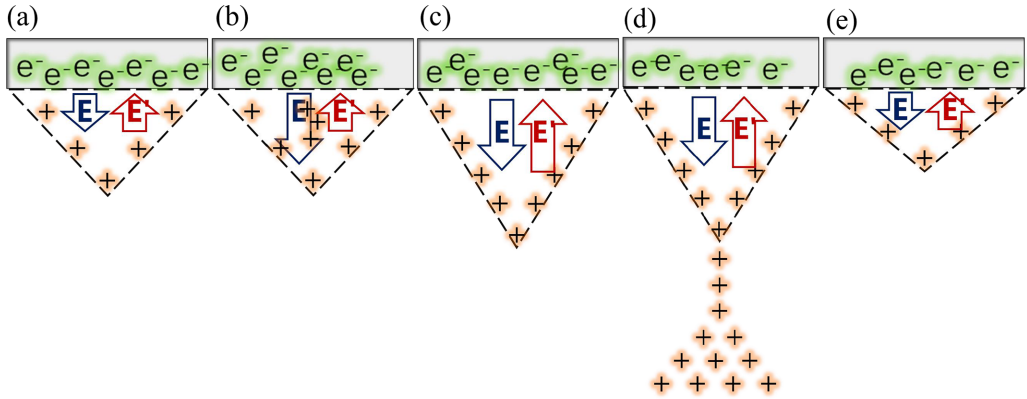


FIG. 8. Diagram of absolute ethyl alcohol diameter oscillation period with pulse height.

The cone is similar to an equipotential body, and the charge is concentrated on the surface of the cone. The charge is excited by an external electric field and flows from the inside of the liquid to the surface of the liquid. The charge distribution has a hysteresis in response to the electric field. In physics, it is considered that the time elapsed when the charge density becomes  $1/e$  of the initial charge density is the charge relaxation time,  $\tau_e$ . The time constant is an inherent property of the fluid, and it measures how fast the charge moves under the action of an electric field [46]. It has nothing to do with the amount of charge, nor does it change with the change of external excitation.

Calculate the charge relaxation time for absolute ethyl alcohol:

$$\tau_{e1} = \frac{\varepsilon_1}{K_1} = \frac{24.1 \times 8.854 \times 10^{-12} \text{ F/m}}{0.003 \text{ } \mu\text{S/cm}} \approx 0.7113 \text{ ms.} \quad (2)$$

The electrical conductivity of the fluid is measured in real time in the experimental environment, and the result shows that the theoretically calculated charge relaxation time is in good agreement with the increasing time of the diameter oscillation obtained by postprocessing the experimental data. (As shown in Fig. 6, the increasing time of the diameter oscillation of absolute ethyl alcohol is 0.7 ms. In fact, the increasing time of the diameter oscillation of absolute ethyl alcohol under all experimental conditions is 0.7 ms, as shown in Appendix A.) Therefore, it is preliminarily believed that the oscillation of the Taylor cone is related to the charge relaxation time under the action of a single pulse voltage. Under a certain DC offset, the meniscus forms a stable Taylor cone, which is an equipotential body. The original electric field and the induced electric field formed by the charge are balanced. The electric field strength inside the cone is zero, and the charge does not move [Fig. 8(a)]. When a single pulse signal is applied, it is equivalent to applying a step voltage, and the strength of the applied electric field increases step by step, which excites a new part of the free charge inside the liquid [Fig. 8(b)]. The internal charge moves to the surface of the liquid, thereby enhancing the induced electric field. The time for the charge to move from the inside to the surface of the liquid is the charge relaxation time  $\tau_e$ . Due to the accumulation of surface charges, the normal electric field force is enhanced, resulting in the elongation of the liquid cone [Fig. 8(c)]. At the same time, the electric charges are also emitted towards the copper plate electrode in the form of atomized droplets [Fig. 8(d)]. The loss of charge reduces the electric field force, and the surface tension dominates, causing the liquid cone to shrink towards the capillary [Fig. 8(e)]. Macroscopically, it is manifested as a decrease in the diameter of the cone tip. As mentioned above, the variation of the diameter oscillation period with the pulse height is reflected only in the descending section of the diameter, which should be related to the amount of charge loss at different pulse heights. Therefore, the trigger connection was used in this study, and the atomization current value under each working condition was collected synchronously. The atomization charge is obtained by integrating the atomization

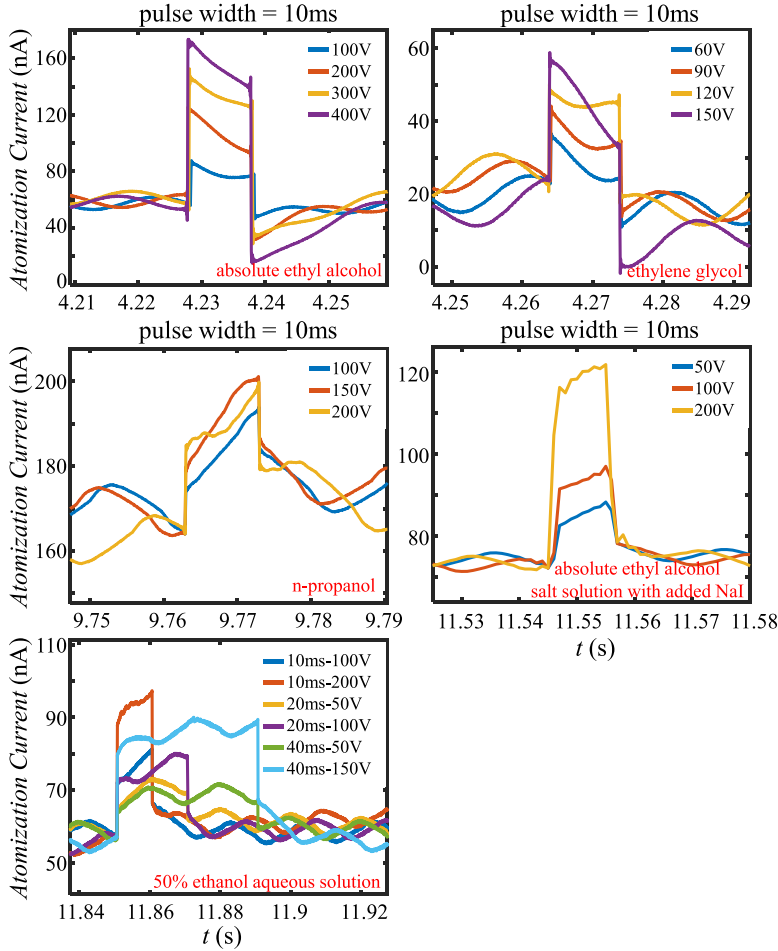


FIG. 9. Atomization current waveform of experimental fluids under single pulse disturbance voltage.

current. Thus, the magnitude of the atomization current directly reflects the amount of charge loss during the application of a single pulse disturbance voltage.

The atomization current value in this paper is obtained by subtracting the average value of the current during the period of not applying a single pulse from the average value of the current during the period of applying a single pulse. The waveform of the atomization current under various working conditions is shown in Fig. 9. Also considering the large amount of data, the atomization current waveforms of the other four fluids under all experimental conditions are shown in Appendix B.

From the atomization current waveforms, it can be intuitively felt that with the increase of the pulse height, the atomization current value indeed increases, and the greater the amount of charge leaving the cone, the greater the difference between the surface tension and the normal electric field force. Thus, the greater the pulse height, the faster the diameter decreases, and the shorter the oscillation period, which is consistent with the experimental results.

The curve of the atomization current value of alcohol fluids with pulse height variation is shown in Fig. 10. Similar to the oscillation period, the atomization voltage current value is related only to the pulse height and does not change with the pulse width. The atomization voltage current value

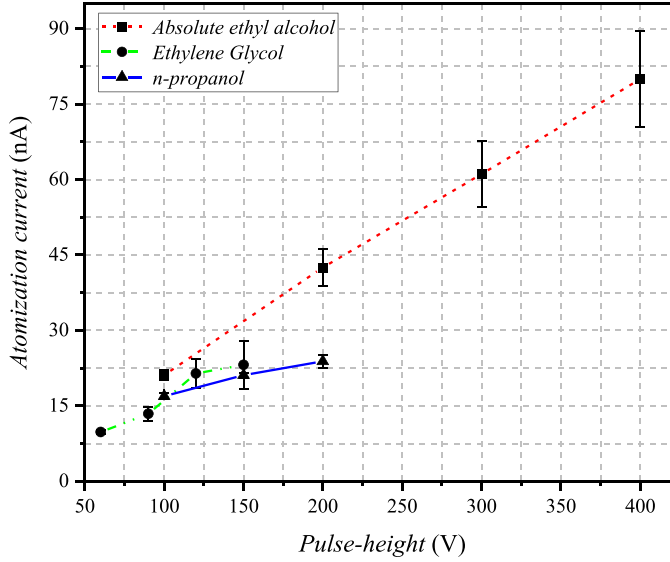


FIG. 10. Diagram of the atomization current of three types of alcohol fluids changing with the pulse height.

reflects the amount of charge leaving the cone. The other two fluids have the same regularity and are not shown in Fig. 10.

In terms of absolute ethyl alcohol, the charge relaxation time was calculated, which is in good agreement with the increasing time of the diameter oscillation. This preliminarily demonstrates the coupling relationship between charge relaxation time and the oscillation time of Taylor cone under a single pulse disturbance voltage. To further verify the oscillation mechanism, the charge relaxation time was also calculated for the other fluids, and compared with the postprocessing data of the experiment (Fig. 6).

Calculate the charge relaxation time for ethylene glycol:

$$\tau_{e2} = \frac{\varepsilon_2}{K_2} = \frac{37 \times 8.854 \times 10^{-12} \text{ F/m}}{0.003 \text{ } \mu\text{S/cm}} \approx 1.092 \text{ ms.} \quad (3)$$

Similarly, the conductivity of ethylene glycol is also the value measured in real time under the experimental environment. The theoretically calculated charge relaxation time of ethylene glycol under the experimental environment is still in good agreement with the increasing time of the diameter oscillation of 1.05 ms.

Calculate the charge relaxation time for *n*-propanol:

$$\tau_{e3} = \frac{\varepsilon_3}{K_3} = \frac{20.1 \times 8.854 \times 10^{-12} \text{ F/m}}{0.002 \text{ } \mu\text{S/cm}} \approx 0.8898 \text{ ms.} \quad (4)$$

The conductivity of *n*-propanol is also the value measured in real time under the experimental environment. The theoretical calculation of the charge relaxation time of *n*-propanol under the experimental environment is still in good agreement with the increasing time of the diameter oscillation of 0.85 ms.

An absolute ethyl alcohol salt solution is prepared by adding 0.0204 g of sodium iodide to 500 ml absolute ethyl alcohol. As can be seen in Table II, after adding a small amount of sodium iodide, the electric field force is obviously enhanced, the opening voltage is significantly reduced under the same nozzle-plate spacing, and the Taylor cone is more likely to rupture under the action of stronger electric field force. For absolute ethyl alcohol, the voltage pulse height reaches 400 V, and the cone surface does not rupture. However, when the pulse height exceeds 200 V under this working

condition, the cone surface has already become unstable and ruptured. As can be seen in Fig. 6, the increasing time of the diameter oscillation of this fluid is a constant value of 1.1 ms, and the addition of inorganic salts will significantly increase the conductivity of the fluid, resulting in a significant decrease in the charge relaxation time of the solution. However, the difference between 1.1 ms and the previous 0.7 ms of absolute ethyl alcohol is very small. Is there any mechanistic error? Subsequently, the conductivity of absolute ethyl alcohol was measured at the ambient temperature of this experiment, and the measurement result was 0.002  $\mu\text{S}/\text{cm}$  (conductivity is extremely sensitive to temperature and requires real time measurement in the experiment), and to calculate the charge relaxation time of absolute ethyl alcohol in this environment:

$$\tau_{e4} = \frac{\varepsilon_4}{K_4} = \frac{24.1 \times 8.854 \times 10^{-12} \text{ F/m}}{0.002 \mu\text{S/cm}} \approx 1.0669 \text{ ms.} \quad (5)$$

$\tau_{e4}$  and  $\tau_{e1}$  both are the charge relaxation time of absolute ethyl alcohol, and due to differences in environmental temperature during the two experiments, the conductivity is different, resulting in a different charge relaxation time. At this time, it is found that the charge relaxation time and the increasing time of the diameter oscillation are still in good agreement, that is, the addition of inorganic salts does not affect the oscillation of the Taylor cone. Therefore, it is speculated that it is not the charge relaxation time of the working fluid that has a strong coupling relationship with the diameter oscillation rise time, but the charge relaxation time of the dielectric component in the fluid, that is, the movement of free ions does not bring about the vibration of the cone surface. What affects the cone oscillation is the movement of charges after polarization. The reason why the aforementioned fluids are in good agreement is that all three types of alcohol fluids are dielectrics.

The 50% ethanol aqueous solution is made by mixing absolute ethyl alcohol and deionized water in equal volume. The formation of the Taylor cone is mainly the result of the competition and balance between the electric field force and the surface tension. Absolute ethyl alcohol, as a fluid that is easier to electrospray, is precisely because of its small surface tension, while the addition of deionized water greatly increases the surface tension of the mixed solution, making it difficult for the Taylor cone to maintain a stable state for a long time. After a single pulse disturbance voltage is applied, the time to maintain a complete cone surface is shorter. Within the limited scope of work, six groups of better experimental conditions were selected for display. As can be seen in Fig. 6, the increasing time of the diameter oscillation of this fluid is a constant value of 1.05 ms, according to the previous conjecture, the increasing time should be the relaxation time of the polarization charge of the dielectric. Is this really the case? The dielectric constant of the mixed solution of this is calculated as the weighted averages based on the volume fraction as  $\varepsilon_{\text{mix}} = 0.5 \times \varepsilon_1 + 0.5 \times \varepsilon_2 = 0.5 \times 24.1 + 0.5 \times 78 = 51.05$ , and uses the DDSJ-308F conductivity meter to measure the conductivity of the mixed solution at this temperature, and the measurement result is 0.004  $\mu\text{S}/\text{cm}$ . From this, the polarization charge relaxation time of the mixed dielectric is calculated:

$$\tau_{e5} = \frac{\varepsilon_5}{K_5} = \frac{51.05 \times 8.854 \times 10^{-12} \text{ F/m}}{0.004 \mu\text{S/cm}} \approx 1.13 \text{ ms.} \quad (6)$$

The calculation results show that this time is in good agreement with the increasing time of the diameter oscillation. Therefore, there is relatively sufficient evidence to prove that the oscillation of the Taylor cone is caused by the charge relaxation phenomenon of the polarization of the dielectric in the solution.

This paper further conducts a parametric analysis based on the well-known Väschi-Buckingham theorem on this issue. The oscillation phenomenon of the Taylor cone under the action of a single pulse voltage is influenced by the physical properties of the fluid, electric field distribution, and flow condition parameters. For the dependent variable, the increasing time of the diameter oscillation, it is affected by eight independent variables: electrical conductivity  $K$ , permittivity  $\varepsilon$ , density  $\rho$ , viscosity  $\mu$ , surface tension coefficient  $\gamma$ , electric field strength  $E$ , nozzle radius  $R$ , and flow rate  $Q$ . The dimensions of the independent and dependent variables are shown in Table IV.

TABLE IV. Dimensions of the independent and dependent variables.

Property	Symbol	Units	Fundamental units
Fising time of the diameter oscillation	$t$	s	$T$
Electrical conductivity	$K$	S/m	$L^{-3}M^{-1}T^3I^2$
Permittivity	$\varepsilon$	$C^2/(N\ m^2)$	$L^{-3}M^{-1}T^4I^2$
Density	$\rho$	$kg/m^3$	$L^{-3}M$
Viscosity	$\mu$	$kg/(m\ s)$	$L^{-1}MT^{-1}$
Surface tension	$\gamma$	N/m	$MT^{-2}$
Electric field intensity	$E$	V/m	$LMT^{-3}I^{-1}$
Nozzle radius	$R$	m	$L$
Flow rate	$Q$	$m^3/s$	$L^3T^{-1}$

Table IV shows that the number of independent variables  $N = 8$ , with the number of basic quantities  $k = 4$  (length  $L$ , mass  $M$ , time  $T$ , current  $I$ ). Using the Väschi-Buckingham theorem for dimensional analysis, it is found that the dimensionless dependent variable  $\Pi$  should be a function of  $N - k = 4$  dimensionless independent variables  $\Pi_1, \Pi_2, \Pi_3, \Pi_4$ , that is

$$\Pi = f(\Pi_1, \Pi_2, \Pi_3, \Pi_4), \quad (7)$$

where the dimensionless independent variable is

$$\Pi = \frac{t}{\varepsilon/K} = \frac{t}{\tau_e}. \quad (8)$$

Based on the governing equations of the Taylor cone [47,48], dimensionless independent variables are selected,

$$\begin{aligned} \Pi_1 &= \frac{\mu}{\sqrt{\rho R \gamma}} = \text{Oh}, \\ \Pi_2 &= \frac{\varepsilon E^2 R}{\gamma} = \text{Bo}_e, \\ \Pi_3 &= \frac{K}{\varepsilon} \sqrt{\frac{\rho R^3}{\gamma}}, \\ \Pi_4 &= \frac{Q \rho K}{\gamma \varepsilon}. \end{aligned} \quad (9)$$

There is a functional relationship as follows:

$$\frac{t}{\varepsilon/K} = f\left(\frac{\mu}{\sqrt{\rho R \gamma}}, \frac{\varepsilon E^2 R}{\gamma}, \frac{K}{\varepsilon} \sqrt{\frac{\rho R^3}{\gamma}}, \frac{Q \rho K}{\gamma \varepsilon}\right). \quad (10)$$

The increasing time of diameter oscillation is strongly coupled with the charge relaxation time, but it is not influenced by this single factor. The above experiments have shown that when the electric field distribution, physical parameters, and flow supply conditions of the fluid are determined, the increasing time of diameter oscillation is strongly correlated with the charge relaxation time of the dielectric in the fluid.

#### IV. CONCLUSION

In this paper the oscillation mechanism of a Taylor cone under a single pulse disturbance voltage is explored experimentally. Five fluid working fluids with different charge relaxation times (absolute

ethyl alcohol, ethylene glycol, *n*-propanol, absolute ethyl alcohol salt solution, and 50% ethanol aqueous solution) are selected. When they form a stable Taylor cone, the single pulse disturbance voltage with different pulse widths and heights is applied respectively. The oscillation timing image of a Taylor cone under this disturbance is captured by a high-speed camera, the atomization current values under various working conditions are collected by using the data acquisition unit, and the following conclusions are obtained.

Under the single pulse disturbance voltage of different pulse widths and heights, the oscillation period of Taylor cone and atomization voltage do not change with the pulse width, but only with the pulse height.

There is a strong coupling relationship between the oscillation of the Taylor cone under a single pulse voltage disturbance and the polarization charge relaxation time of the dielectric in the fluid. The diameter oscillation at a fixed position of the Taylor cone has an invariant, that is, the rise time of the diameter oscillation, which is in good agreement with the polarization charge relaxation time of the fluid.

#### ACKNOWLEDGMENT

This work was supported by the National Natural Science Foundation of China (Grant No. 12272026).

#### APPENDIX A

The postprocessing diameter oscillation diagrams for the complete experimental conditions are shown in this Appendix.

The diameter at a fixed position of the cone tip is extracted to obtain the diameter oscillation diagram of absolute ethyl alcohol under different pulse widths and heights, as shown in Fig. 11. For ethylene glycol, it is shown in Fig. 12. For *n*-propanol, it is shown in Fig. 13. For an absolute ethyl alcohol salt solution with added NaI, it is shown in Fig. 14. For a 50% ethanol aqueous solution, it is shown in Fig. 15.

#### APPENDIX B

The atomization current waveforms of the experimental fluids under all experimental conditions are shown in this Appendix.

The atomization current value in this paper is obtained by subtracting the average value of the current during the period of not applying a single pulse from the average value of the current during the period of applying a single pulse. The atomization current waveform of absolute ethyl alcohol under various working conditions is shown in Fig. 16. For ethylene glycol, it is shown in Fig. 17. For *n*-propanol, it is shown in Fig. 18. For an absolute ethyl alcohol salt solution with added NaI, it is shown in Fig. 19. For a 50% ethanol aqueous solution, it is shown in Fig. 20.



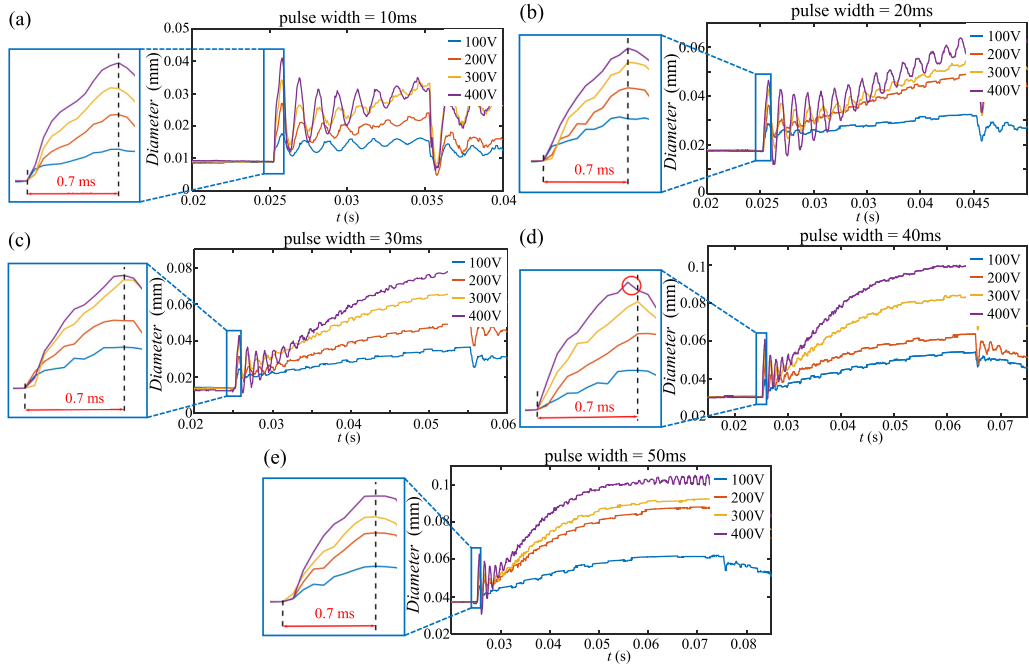


FIG. 11. Diameter oscillation diagram of absolute ethyl alcohol under different pulse heights when the pulse width is (a) 10 ms, (b) 20 ms, (c) 30 ms, (d) 40 ms, and (e) 50 ms.

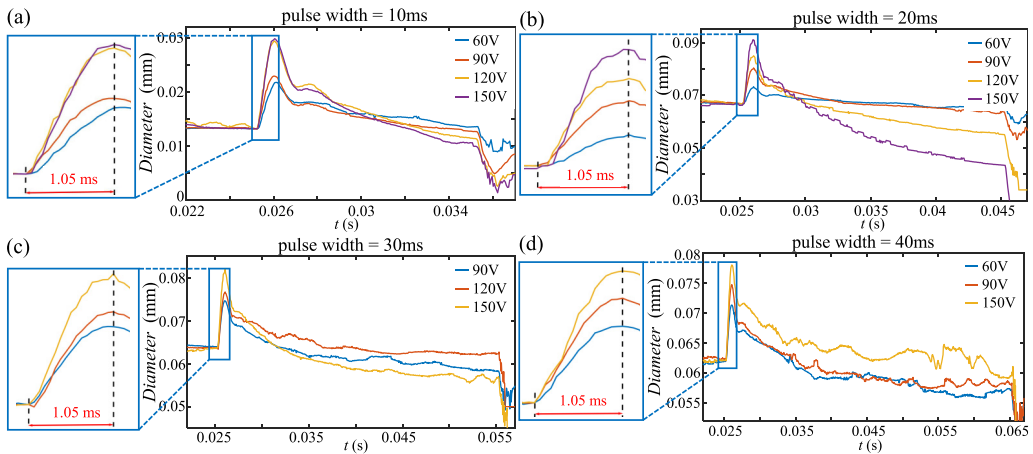


FIG. 12. Diameter oscillation diagram of ethylene glycol under different pulse heights when the pulse width is (a) 10 ms, (b) 20 ms, (c) 30 ms, and (d) 40 ms.

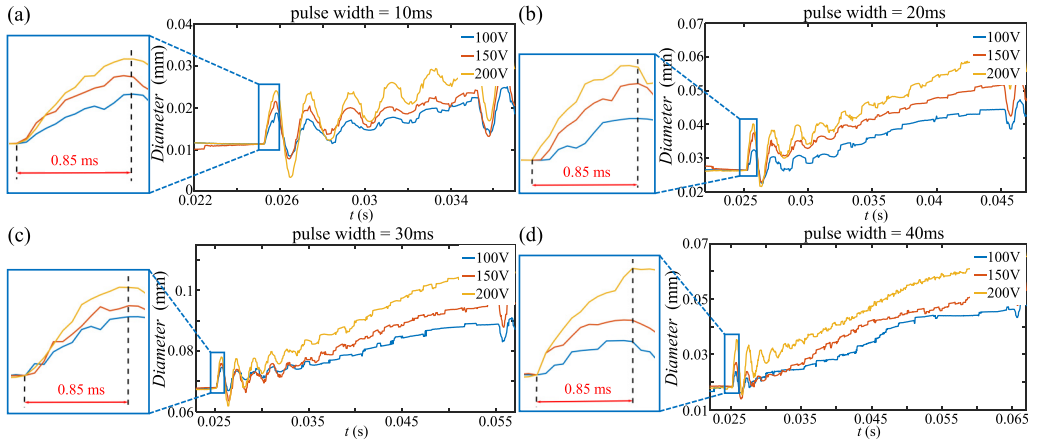


FIG. 13. Diameter oscillation diagram of *n*-propanol under different pulse heights when the pulse width is (a) 10 ms, (b) 20 ms, (c) 30 ms, (d) 40 ms.

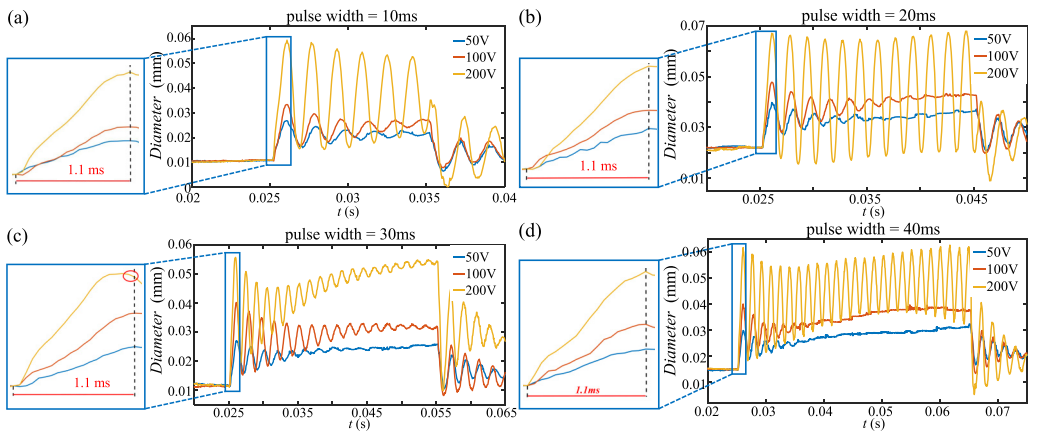


FIG. 14. Diameter oscillation diagram of absolute ethyl alcohol salt solution under different pulse heights when the pulse width is (a) 10 ms, (b) 20 ms, (c) 30 ms, (d) 40 ms.

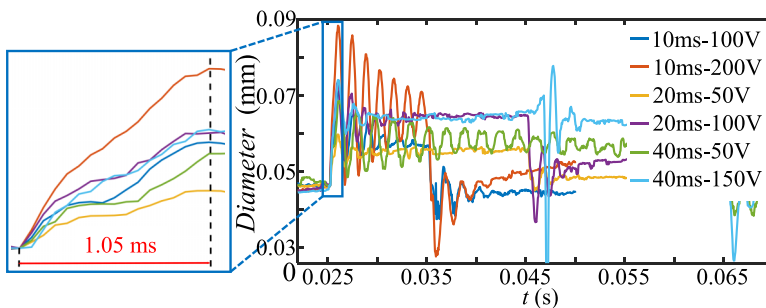


FIG. 15. Diameter oscillation diagram of a 50% ethanol aqueous solution under different pulse widths and heights.

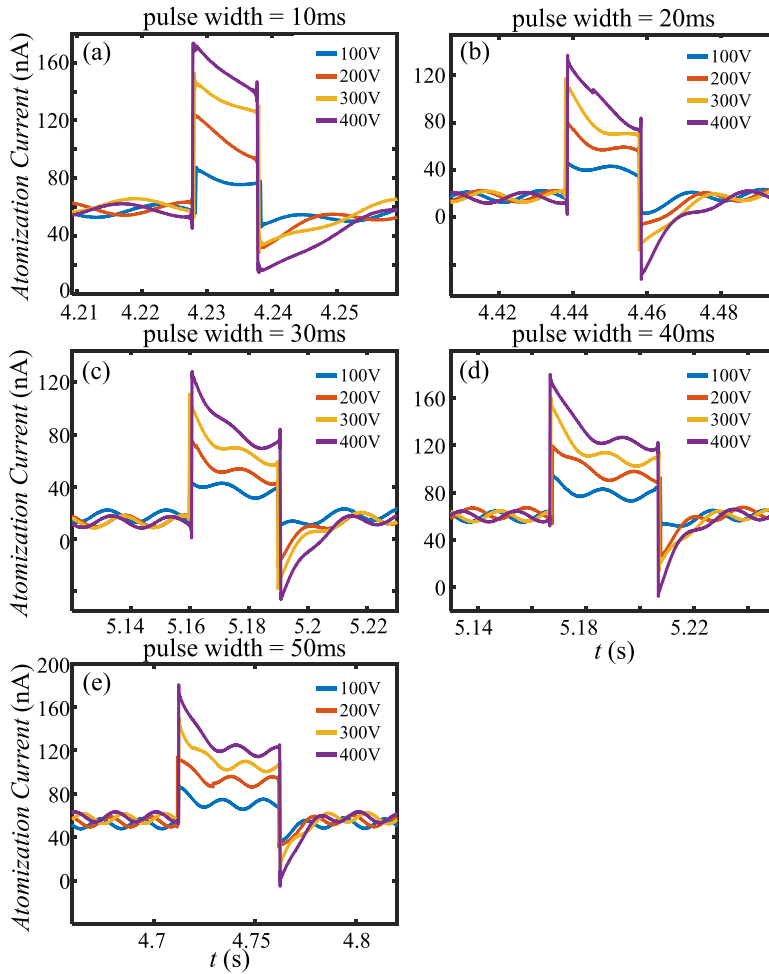


FIG. 16. Atomization current waveform of absolute ethyl alcohol under different pulse heights when the pulse width is (a) 10 ms, (b) 20 ms, (c) 30 ms, (d) 40 ms, and (e) 50 ms.

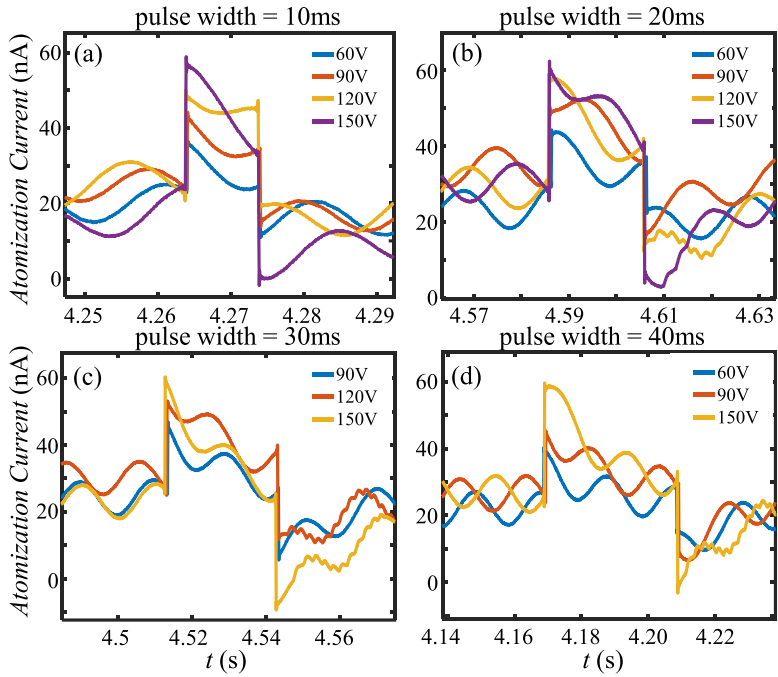


FIG. 17. Atomization current waveform of ethylene glycol under different pulse heights when the pulse width is (a) 10 ms, (b) 20 ms, (c) 30 ms, and (d) 40 ms.

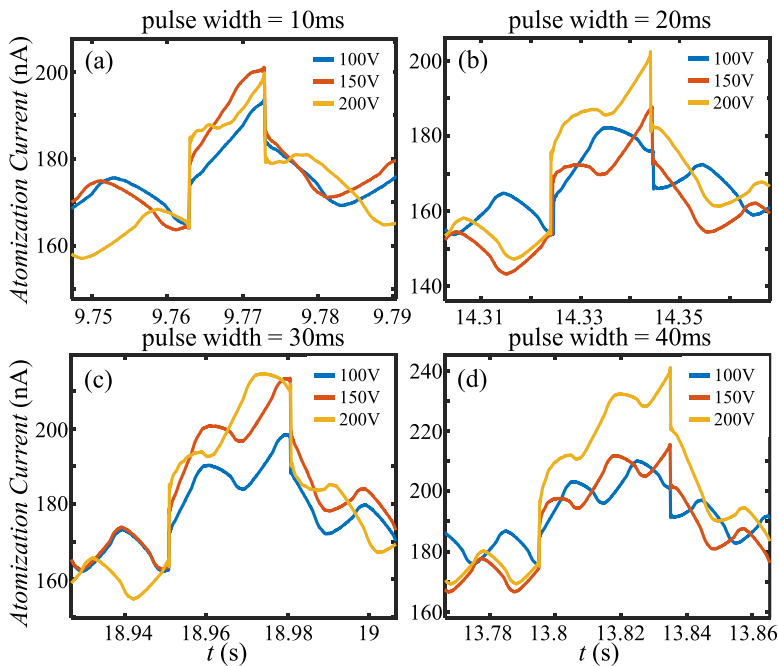


FIG. 18. Atomization current waveform of *n*-propanol under different pulse heights when the pulse width is (a) 10 ms, (b) 20 ms, (c) 30 ms, (d) 40 ms.

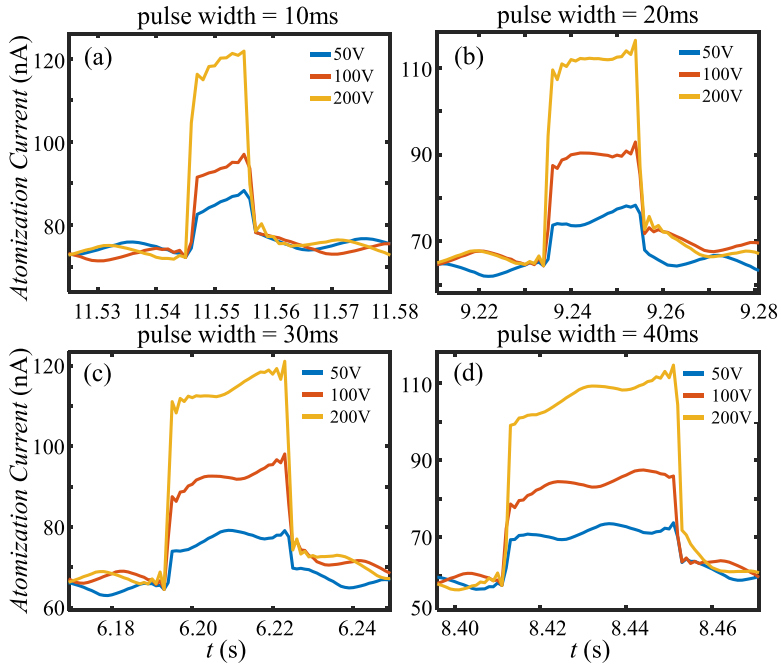


FIG. 19. Atomization current waveform of an absolute ethyl alcohol salt solution under different pulse heights when the pulse width is (a) 10 ms, (b) 20 ms, (c) 30 ms, (d) 40 ms.

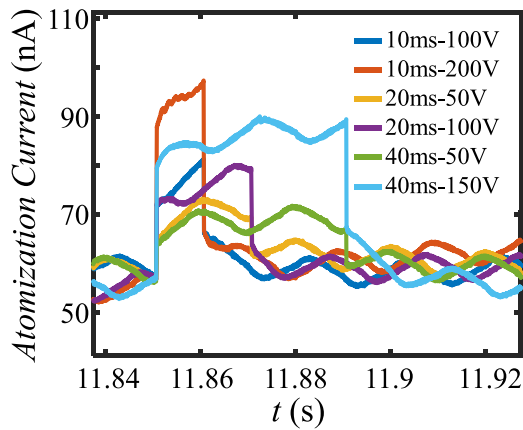


FIG. 20. Atomization current waveform of a 50% ethanol aqueous solution under different pulse widths and heights.

- [1] A. Jaworek, M. Lackowski, A. Krupa, and T. Czech, Electrostatic interaction of free EHD jets, [Exp. Fluids](#) **40**, 568 (2006).
- [2] S. Dandavino, C. Ataman, S. Chakraborty, H. Shea, C. Ryan, and J. Stark, Progress towards a miniaturized electrospray thruster for propulsion of small spacecraft, in *Proceedings of the 48th AIAA/ASME/SAE/ASEE Joint Propulsion Conference & Exhibit* (AIAA Press, Reston, VA, 2012).
- [3] T. Henning, K. Huhn, L. W. Isberner, and P. J. Klar, Miniaturized electrospray thrusters, [IEEE Trans. Plasma Sci. Trans. Plasma Sci.](#) **46**, 214 (2018).
- [4] M. S. Alexander, J. Stark, K. L. Smith, B. Stevens, and B. Kent, Electrospray performance of microfabricated colloid thruster arrays, [J. Propul. Power](#) **22**, 620 (2006).
- [5] A. R. H. Rigit and J. S. Shrimpton, Electrical performance of charge injection electrostatic atomizers, [Atomization Sprays](#) **16**, 401 (2006).
- [6] J. Xie, J. Jiang, P. Davoodi, M. Srinivasan, and C.-H. Wang, Electrohydrodynamic atomization: A two-decade effort to produce and process micro-/nanoparticulate materials, [Chem. Eng. Sci.](#) **125**, 32 (2015).
- [7] Q. Dumont and R. B. Cole, Jean-Antoine Nollet: The father of experimental electrospray, [Mass Spectrom. Rev.](#) **33**, 418 (2014).
- [8] J. W. S. B. Rayleigh, *The Theory of Sound* (Macmillan & Company, New York, 1896), Vol. 2.
- [9] C. Garton and Z. Krasucki, Bubbles in insulating liquids: Stability in an electric field, [Proc. R. Soc. London A](#) **280**, 211 (1964).
- [10] G. I. Taylor, Disintegration of water drops in an electric field, [Proc. R. Soc. London A](#) **280**, 383 (1964).
- [11] J. Zeleny, Instability of electrified liquid surfaces, [Phys. Rev.](#) **10**, 1 (1917).
- [12] C. J. Angamma and S. H. Jayaram, The effects of electric field on the multijet electrospinning process and fiber morphology, [IEEE Trans. Ind. Appl.](#) **47**, 1028 (2011).
- [13] M. A. Herrada, J. M. López-Herrera, A. M. Gañán-Calvo, E. J. Vega, J. M. Montanero, and S. Popinet, Numerical simulation of electrospray in the cone-jet mode, [Phys. Rev. E](#) **86**, 026305 (2012).
- [14] M. Gamero-Castaño and M. Magnani, Numerical simulation of electrospaying in the cone-jet mode, [J. Fluid Mech.](#) **859**, 247 (2019).
- [15] F. Cruz-Mazo, M. O. Wiedorn, M. A. Herrada, S. Bajt, H. N. Chapman, and A. M. Gañán-Calvo, Aerodynamically stabilized taylor cone jets, [Phys. Rev. E](#) **100**, 031101(R) (2019).
- [16] C. Li, M. Chang, W. Yang, A. Madden, and W. Deng, Ballpoint pen tips as robust cone-jet electrospray emitters, [J. Aerosol Sci.](#) **77**, 10 (2014).
- [17] M. R. Morad, A. Rajabi, M. Razavi, and S. R. P. Sereshkeh, A very stable high throughput taylor cone-jet in electrohydrodynamics, [Sci. Rep.](#) **6**, 38509 (2016).
- [18] M. Gamero-Castaño and M. Magnani, The minimum flow rate of electrosprays in the cone-jet mode, [J. Fluid Mech.](#) **876**, 553 (2019).
- [19] A. M. Gañán-Calvo and J. M. Montanero, Self-similar electrohydrodynamic solutions in multiple coaxial Taylor cones, [J. Fluid Mech.](#) **915**, R1 (2021).
- [20] Z. Wang, Y. Tian, C. Zhang, Y. Wang, and W. Deng, Massively multiplexed electrohydrodynamic tip streaming from a thin disc, [Phys. Rev. Lett.](#) **126**, 064502 (2021).
- [21] L. L. F. Agostinho, C. U. Yurteri, E. C. Fuchs, and J. C. M. Marijnissen, Monodisperse water microdroplets generated by electrohydrodynamic atomization in the simple-jet mode, [Appl. Phys. Lett.](#) **100**, 244105 (2012).
- [22] Z. Jiang, Y. Gan, and Y. Shi, An improved model for prediction of the cone-jet formation in electrospray with the effect of space charge, [J. Aerosol Sci.](#) **139**, 105463 (2020).
- [23] L. Rayleigh, On the equilibrium of liquid conducting masses charged with electricity, [London Edinburgh Dublin Philos. Mag. J. Sci.](#) **14**, 184 (1882).
- [24] G. I. Taylor, Electrically driven jets, [Proc. R. Soc. London A](#) **313**, 453 (1969).
- [25] P. Son and K. Ohba, Theoretical and experimental investigations on instability of an electrically charged liquid jet, [Int. J. Multiphase Flow](#) **24**, 605 (1998).
- [26] D. A. Saville, Electrohydrodynamic stability: Fluid cylinders in longitudinal electric fields, [Phys. Fluids](#) **13**, 2987 (1970).

- [27] J. R. Melcher and G. I. Taylor, Electrohydrodynamics: A review of the role of interfacial shear stresses, *Annu. Rev. Fluid Mech.* **1**, 111 (1969).
- [28] R. T. Collins, J. J. Jones, M. T. Harris, and O. A. Basaran, Electrohydrodynamic tip streaming and emission of charged drops from liquid cones, *Nat. Phys.* **4**, 149 (2008).
- [29] Y. Guan, S. Wu, M. Wang, Y. Tian, C. Yu, W. Lai, and Y. Huang, Numerical investigation of high-frequency pulsating electrohydrodynamic jet at low electric Bond numbers, *Phys. Fluids* **34**, 012001 (2022).
- [30] Y. Guan, S. Wu, M. Wang, Y. Tian, W. Lai, and Y. Huang, Numerical analysis of electrohydrodynamic jet printing under constant and step change of electric voltages, *Phys. Fluids* **34**, 062005 (2022).
- [31] K. Mohammadi, M. R. Movahhedy, and S. Khodaygan, A multiphysics model for analysis of droplet formation in electrohydrodynamic 3D printing process, *J. Aerosol Sci.* **135**, 72 (2019).
- [32] A. Jaworek, W. Machowski, A. Krupa, and W. Balachandran, Viscosity effect on EHD spraying using AC superimposed on DC electric field, in *Conference Record of the 2000 IEEE Industry Applications Conference. Thirty-Fifth IAS Annual Meeting and World Conference on Industrial Applications of Electrical Energy (Cat. No. 00CH37129)* (IEEE, New York, 2000), Vol. 2, pp. 770–776.
- [33] L. Y. Yeo, D. Lastochkin, S.-C. Wang, and H.-C. Chang, A new ac electro spray mechanism by Maxwell-Wagner polarization and capillary resonance, *Phys. Rev. Lett.* **92**, 133902 (2004).
- [34] L. Y. Yeo, Z. Gagnon, and H.-C. Chang, AC electro spray biomaterials synthesis, *Biomaterials* **26**, 6122 (2005).
- [35] A. M. Gañán-Calvo, J. M. López-Herrera, M. A. Herrada, A. Ramos, and J. M. Montanero, Review on the physics of electro spray: From electrokinetics to the operating conditions of single and coaxial Taylor cone-jets, and AC electro spray, *J. Aerosol Sci.* **125**, 32 (2018).
- [36] J. M. López-Herrera, M. A. Herrada, and A. M. Gañán-Calvo, Electrokinetic modelling of cone-jet electro sprays, *J. Fluid Mech.* **964**, A19 (2023).
- [37] A. M. Gañán-Calvo, The surface charge in electro spraying: Its nature and its universal scaling laws, *J. Aerosol Sci.* **30**, 863 (1999).
- [38] S. Faraji, B. Sadri, B. V. Hokmabad, N. Jadidoleslam, and E. Esmaeilzadeh, Experimental study on the role of electrical conductivity in pulsating modes of electro spraying, *Exp. Thermal Fluid Sci.* **81**, 327 (2017).
- [39] J.-B. Cheng, L.-J. Yang, Q.-F. Fu, J.-X. Ren, H.-B. Tang, D.-K. Sun, and X.-F. Sun, Pulsating modes of a Taylor cone under an unsteady electric field, *Phys. Fluids* **34**, 012007 (2022).
- [40] E. Lyvers, O. Mitchell, M. Akey, and A. Reeves, Subpixel measurements using a moment-based edge operator, *IEEE Trans. Pattern Anal. Machine Intell.* **11**, 1293 (1989).
- [41] J. A. Christian, Accurate planetary limb localization for image-based spacecraft navigation, *J. Spacecr. Rockets* **54**, 708 (2017).
- [42] S. Ghosal and R. Mehrotra, Orthogonal moment operators for subpixel edge detection, *Pattern Recogn.* **26**, 295 (1993).
- [43] S. Ghosal and R. Mehrotra, Detection of composite edges, *IEEE Trans. Image Process.* **3**, 14 (1994).
- [44] S. Ghosal and R. Mehrotra, A moment-based unified approach to image feature detection, *IEEE Trans. Image Process.* **6**, 781 (1997).
- [45] J. Canny, A computational approach to edge detection, *IEEE Trans. Pattern Anal. Mach. Intell.* **PAMI-8**, 679 (1986).
- [46] *Electrohydrodynamics*, edited by A. Castellanos (Springer Vienna, Vienna, 1998).
- [47] E. Buckingham, On physically similar systems; illustrations of the use of dimensional equations, *Phys. Rev.* **4**, 345 (1914).
- [48] A. Ponce-Torres, N. Rebollo-Muñoz, M. A. Herrada, A. M. Gañán-Calvo, and J. M. Montanero, The steady cone-jet mode of electro spraying close to the minimum volume stability limit, *J. Fluid Mech.* **857**, 142 (2018).